Journal of Membrane Science 595 (2020) 117521

Contents lists available at ScienceDirect

Journal of Membrane Science

journal homepage: http://www.elsevier.com/locate/memsci

Dual hydrophobic modifications toward anion exchange membranes with both high ion conductivity and excellent dimensional stability

Chuan Hu, Qiugen Zhang *, Hongyue Wu, Xiuli Deng, Qian Yang, Peng Liu, Yanzhen Hong, Aimei Zhu, Qinglin Liu

Department of Chemical and Biochemical Engineering, College of Chemistry and Chemical Engineering, Xiamen University, Xiamen, 361005, China

ARTICLE INFO

Keywords:
Anion exchange membrane
Trade-off relation
Hydrophobic modification
Crosslinked membrane
H_2/O_2 fuel cell

ABSTRACT

Anion exchange membrane (AEMs) as a kind of important functional material are widely used in many fields including fuel cell, electrodialysis and water treatment. However, synthetic AEMs generally suffer a pernicious trade-off: high ion-conductive AEMs lack dimensional stability and vice versa. Herein we demonstrate a versatile strategy to prepare the AEMs with both high ion conductivity and excellent dimensional stability (*i.e.*, low swelling ratio) *via* hydrophobic crosslinking and introducing hydrophobic chains. The hydrophobic length of crosslinkers has great influence on construction of highly efficient ion channels in the AEMs. Amazingly, the hydrophilic poly (phenylene oxide) (PPO) AEM crosslinked by 1,8-diaminooctane has the highest hydroxide conductivity that is further improved to 157.2 mS cm^{-1} (10% increases) with a low swelling ratio of 12.9% at 80 °C by introducing hydrophobic PPO backbone. This AEM not only overcomes the trade-off between the ion conductivity and the dimensional stability of crosslinked AEMs, but also breaks the upper bound between the ion conductivity and the water uptake. The newly developed strategy of hydrophobic dual-modifications promises to be an effective approach to develop the high-performance AEMs.

1. Introduction

Anion exchange membrane fuel cell (AEMFCs) have attracted a growing interest in past decades due to its nonnegligible advantages comparing with proton exchange membranes (PEMFCs) [1-3]. Under alkaline conditions, there is a higher active electronic reaction and faster reaction rate in AEMFCs which allow non-precious metal as catalysts [4,5]. Anion exchange membranes (AEMs) as the core module of AEMFC directly determine the performance of AEMFCs, including the longevity of fuel cell and power density [6,7]. An ideal AEM should equipped with the high anion conductivity, robust mechanical property and excellent alkaline stability under high pH conditions [8-11]. However, until now, the developed AEMs could not fully meet the increasing requirements of this fields. Specially, these AEMs often suffer insufficient alkaline stability and the trade-off between ion conductivity and the dimensional stability in working environment [12-14].

The ion conductivity is one of important properties of AEMs to determine the performance of fuel cells [15,16]. To improve the ion conductivity, a general method is to increase ion exchange capacity (IEC) of the AEMs, which reflects the ability to exchange ion [17]. However, the high IEC cause a large swelling of the AEMs in water surrounding, resulting in a low dimensional stability (*i.e.*, great swelling ratio) that is undesirable for the fuel cell. To overcome this trade-off between the ion conductivity and the dimensional stability, various AEMs were developed in past decades, such as side-chain-type AEMs, block-type AEMs and crosslinked AEMs [5,18-22]. Among them, the crosslinked AEMs are the most popular one due to their simple operation, and can be accomplished *via* thermal treatment, UV radiation or introduction of crosslinkers. The former two methods are performed in the polymers equipped with double carbon bond, triple carbon bond or other active groups, whereas the latter by reaction between backbone and crosslinker [9,23-26].

Nowadays, researchers prefer hydrophilic crosslinkers to modify the AEMs because they give a chance to restrict the swelling and improve the ion conductivity simultaneously. For instance, ether-containing crosslinker improved the water uptake and the ion conductivity of chloromethylated aromatic polymer-based AEMs [27], the multi-cation crosslinkers largely improved the ion conductivity of Tröger's base copolymer AEMs due to introduction of additional cationic groups [28]. In general, the AEMs require the high IEC to obtain the high ion

* Corresponding author.
E-mail address: qgzhang@xmu.edu.cn (Q. Zhang).

https://doi.org/10.1016/j.memsci.2019.117521
Received 25 June 2019; Received in revised form 22 September 2019; Accepted 28 September 2019
Available online 28 September 2019
0376-7388/© 2019 Elsevier B.V. All rights reserved.

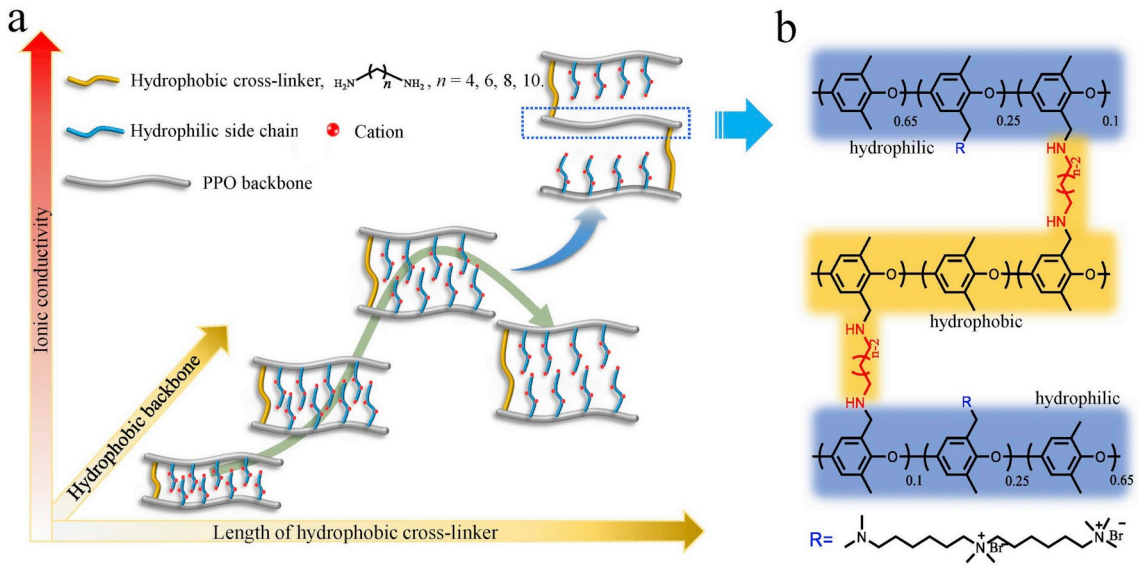

Fig. 1. Preparation of high-performance AEMs *via* the dual hydrophobic modifications. (a) Schematic for the dual hydrophobic modifications. (b) Chemical structure of PPO-based AEMs prepared by the dual hydrophobic modifications.

conductivity. In this case, the hydrophilic crosslinkers cannot effectively depress the swelling of the AEMs, resulting in low dimensional stability. For instance, the polyisopreneran-poly (vinyl benzyl trimethyl ammonium chloride) AEM crosslinked by 2,2'-(ethylenedioxy) diethanethiol could not keep intact to measure the ion conductivity when the IEC is over 1.66 mmol g^{-1} [29]. Therefore, a more effective crosslinking approach is required to control the swelling of the AEM with the high IEC.

Recently, hydrophobic crosslinking has been attracted increasing attention due to its excellent anti-swelling ability [30,31]. For instance, the swelling ratio of triblock copolymer AEM decreases from 137 to 22% after crosslinking by 1,10-decanedithiol [32]. The cationic poly (ether sulfone) membrane has the low swelling ratio of 9.2% (30 °C) after crosslinking between trifluorovinyl groups [30]. Moreover, the PPO-based copolymer, crosslinked by hydrophobic long-side chain *via* olefin metathesis, exhibits the low swelling ratio of 5.4% (30 °C) [33]. Although the hydrophobic crosslinking shows a great potential to improve the dimensional stability of AEMs, however the formed AEMs with the moderate ion conductivity cannot meet the requirement for the fuel cell. Therefore, a more efficient hydrophobic modification is strongly required for the preparation of AEMs with the high ion conductivity and the low swelling ratio.

In this paper, we demonstrated a versatile strategy to prepare the high-performance AEMs by combining both the hydrophobic crosslinker and the hydrophobic chain, as shown in Fig. 1a. The hydrophilic PPO (HPPO) with the IEC of 3.05 mmol g^{-1} was used as the AEM matrix due to advantages (*e.g.*, high chemical stability, easy modification and low-cost) of PPO [34,35]. Alkyl diamines with different length were used as the hydrophobic crosslinkers to modify the HPPO AEMs. Unlike tertiary diamine-based crosslinkers, primary diamine-based crosslinkers do not form quaternary ammonium salts that are easily to degrade under alkaline environment, and can perform the crosslinking reaction under milder reaction conditions [36,37]. The crosslinked AEMs were further modified by introducing hydrophobic PPO chains. The as-formed PPO-based AEMs have both the hydrophobic crosslinkers and the hydrophobic PPO chains (Fig. 1b), and thus are expected to own the high

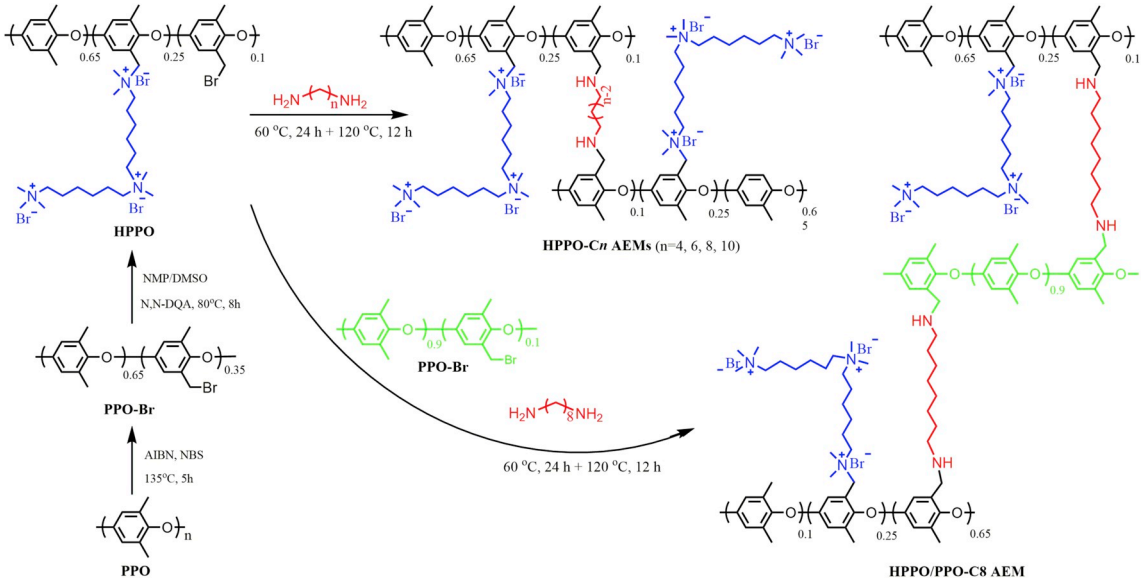

Fig. 2. Synthetic routes for HPPO, HPPO-C*n* AEMs and HPPO/PPO-C8 AEM.

ion conductivity and the good dimensional stability. Microstructure, physicochemical properties and fuel cell performance of as-prepared AEMs were studied in details.

2. Experimental

2.1. Materials

PPO with the density of 1.06 g mL^{-1} (25 °C) was purchased from *Sigma-Aldrich*. The alkyl diamines including 1,4-diaminbutane (C4), 1,6-hexamethylenediamine (C6), 1,8-diaminooctane (C8) and 1,10-diaminodecane (C10) were purchased from *Shanghai Macklin Biochemical Co. Ltd*. *N*-bromosuccinimide (NBS) and azobisisobutyronitrile (AIBN) were purchased from *Aladdin Industrial Inc*. and *J&K Scientific Co. Ltd*, respectively. Solvents including N-methyl pyrrolidone (NMP), dimethyl sulfoxide (DMSO), chlorobenzene, diethyl ether and methanol were purchased from Shanghai *Sinopharm Chemical Reagent Co. Ltd*. All reagents were used without further purification.

2.2. Preparation of HPPO-Cn and HPPO/PPO-C8 AEMs

As depicted in Fig. 2, the HPPO was synthesized first *via* brominating and grafting processes [38]. Typically, 12.00 g (100 mmol) PPO and 100 mL chlorobenzene were added in a dried 250 mL three-necked flask equipped with a condenser, magnetic stirrer and nitrogen atmosphere. After dissolved completely, 8.90 g (50 mmol) NBS and 0.50 g (3 mmol) AIBN were added to the mixture and then stirred at 135 °C for 5 h. Subsequently, the mixture was cooled down to the room temperature and precipitated in methanol. The resulting precipitation was filtered and washed with methanol for three times. The brominated PPO (labelled as PPO-Br) with the brominating degree of 0.35 was obtained. After that, 3.00 g PPO-Br (20 mmol) and 2.40 g N^1-(6-(dimethylamino) hexyl)-N^1,N^1,N^6,N^6,N^6-pentamethylhexane-1,6-diaminium bromide (*N,N*-DQA) (5 mmol) were dissolved in 40 mL NMP and 20 mL DMSO, respectively. Then, the *N,N*-DQA solution was slowly added into the PPO-Br solution. The resulting mixture was stirred at 60 °C for 24 h and then precipitated in diethyl ether. Finally, the HPPO was obtained after washing with diethyl ether for three times and drying under vacuum at 80 °C for 24 h. The ^{1}H NMR spectra of PPO-Br and HPPO were recorded by Bruker Avance II 400 MHz using $CDCl_3$ as the solvent and tetramethysilane (TMS) as an internal reference.

The crosslinked HPPO AEMs (labelled as HPPO-C*n*, *n* is the number of carbon atoms in the alkyl) were prepared by using alkyl diamines with the different length of alkyl (C4, C6, C8 and C10) as the hydrophobic crosslinkers, as depicted in Fig. 2. Typically, 0.20 g HPPO (0.7734 mmol) was dissolved in 5 mL NMP to form a clear solution. Then, the alkyl diamines (0.0386 mmol) was added under stirring. The resulting solution was cast onto a glass plate and placed into a vacuum oven at 60 °C for 24 h and 120 °C for another 12 h to remove residual solvent. The formed HPPO-C*n* AEMs in Br form were immersed in 1 M NaOH solution for 24 h to exchange Br with OH. After that, the AEMs were immersed in the deionized water (after ultrasonic treatment for 2 h at 60 °C) for three times to remove residual alkali. For the HPPO/PPO-C8 AEM, 0.0326 g PPO-Br (0.2209 mmol) were dissolved in 5 mL NMP to form a clear solution. Subsequently, 0.0111 g (0.0773 mmol) 1,8-diaminooctane was added into the mixed solution. Then, the HPPO/PPO-C8 AEM was obtained by the same preparing process of HPPO-C*n* AEMs.

2.3. Characterizations of physicochemical structure of AEMs

Physicochemical structure of prepared PPO-based AEMs was demonstrated by their Fourier transform infrared spectroscopy (FT-IR) spectra, thermal stability, mechanical properties, gel fraction and density. The FT-IR spectra was recorded on a Nicolet Avatar 380 spectrophotometer (Thermo Electron Corporation, USA). The thermal stability was measured by a simultaneous TGA/DSC system (SDT Q600, TA Instruments Waters LLC, USA) under a nitrogen flow (100 mL min^{-1}) with a heating rate of 10 °C min^{-1} in the range of 30–800 °C. The mechanical properties were measured by a universal testing machine (Instron 3343) with a stretching rate of 0.25 mm min^{-1}. Before testing, the AEMs were immersed in the deionized water at the room temperature for 24 h and dried in the vacuum oven at 80 °C for 24 h, respectively. The dried and wet samples were cut into the shape of dog-bone with the effective area of 20 mm × 2 mm.

The gel fraction was used to characterize the crosslinked degree of AEMs. A rectangular AEM sample was dried under vacuum at 100 °C for 24 h to remove residual water and the weight was recorded as m_1. After that, the sample was immersed in the NMP solution at 80 °C for 24 h to remove the soluble component. Finally, the sample was taken out and dried under vacuum at 100 °C for 24 h to remove the residual NMP. The mass was measured as m_2. The gel fraction of AEMs was calculated by

$$\text{Gel fraction} = \frac{m_2}{m_1} \times 100\% \quad (1)$$

The density of the AEMs was measured by a digital microbalance (Mettler Toledo, AB204-S) with density kit at 25 °C. Before measuring, the AEMs were dried under vacuum at 100 °C for 24 h to remove residual water and the weight was recorded as m_1. After that, the AEMs were immersed in toluene to measure its mass recorded m_2. The density (ρ) of AEMs was calculated by

$$\rho = \frac{m_1 \rho_{toluene}}{m_1 - m_2} \quad (2)$$

where $\rho_{toluene}$ is the density of toluene at 25 °C.

2.4. Observation of morphology and microstructure of AEMs

Morphology and microstructure of prepared PPO-based AEMs were observed by atomic force microscopy (AFM) (5500, Agilent Technologies, USA), small angle X-ray scattering (SAXS) (SAXSess-mc2, Anton Paar, Austria) and transmission electron microscopy (TEM) (JEM-2100, JEM Ltd. Japan). The AFM samples were prepared as following: taking 0.2 mL mixture solution (HPPO and crosslinkers) dropped into mica and then dried under vacuum 60 °C for 24 h and 120 °C for another 12 h. The phase images were obtained by Multimode V microscope (Bruker Co. Germany) under the tapping mode. The TEM samples were prepared according to the previous work [28]. The membranes in the Br^- form were immersed in 1 M Na_2WO_4 solution for 48 h to exchange Br^- with WO_4^{2-}. Then, the samples were washed with deionized water to remove residual Na_2WO_4, and dried under vacuum at 60 °C for 24 h before embedded in epoxy resin. Finally, the samples were cut into thin slice through ultramicrotome, which were collected in copper grid.

2.5. Swelling experiments of AEMs

A rectangular AEM sample in the OH form was dried under vacuum at 80 °C for 24 h to remove bound water, and then immersed in the deionized water at different temperatures for 24 h to reach the swelling equilibrium. The swollen sample was taken out and quickly wiped with filter papers to remove excessive surface water. The water uptake (%) and swelling ratio (%) were calculated by

$$\text{Water uptake} = \frac{m_{swollen} - m_{dry}}{m_{dry}} \times 100\% \quad (3)$$

$$\text{Swelling ratio} = \frac{l_{swollen} - l_{dry}}{l_{dry}} \times 100\% \quad (4)$$

where m_{dry} and l_{dry} is the mass and length of dry samples. $M_{swollen}$ and $l_{swollen}$ is the mass and length of swollen samples.

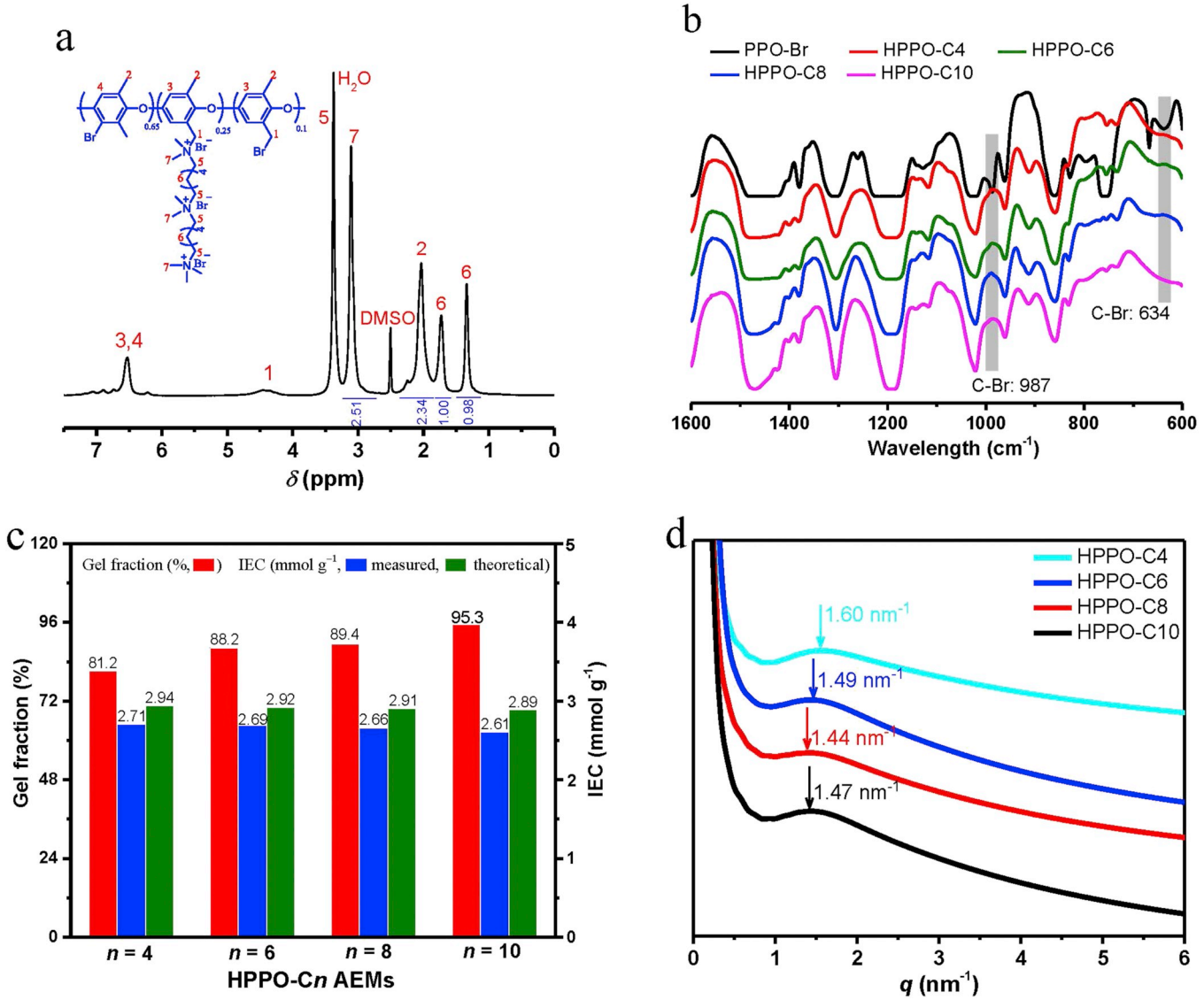

Fig. 3. Physicochemical structure of HPPO-C*n* AEMs ($n = 4, 6, 8, 10$). (b) The ^{1}H NMR spectrum of HPPO. (b) FT-IR spectra of PPO-Br and HPPO-C*n* AEMs. (c) The gel fraction and IEC of HPPO-C*n* AEMs. (d) SAXS profiles of HPPO-C*n* AEMs (The *d*-spacing is calculated according to Bragg equation).

2.6. Measurements of IEC and ion conductivity of the AEMs

The IEC was measured by titration. The sample in the Br form was dried to a constant weight (M_{dry}) under vacuum at 100 °C. Subsequently, the dry samples were immersed in 0.15 M $NaNO_3$ solution (20 mL) at 30 °C for 48 h to release Br completely. Finally, the above solution was titrated with $AgNO_3$ solution using K_2CrO_4 as indicator. The IEC was calculated by

$$\mathrm{IEC} = \frac{C_{AgNO_3} \times V_{AgNO_3}}{M_{dry}} \times 100\% \quad (5)$$

where C_{AgNO_3} and V_{AgNO_3} is the concentration and volume of $AgNO_3$ solution, respectively.

The hydroxide conductivity of AEMs was measured by an electrochemical workstation (Versa STAT 4, USA) using four-point probe alternating current (AC) technology in the range of 30–80 °C with an interval of 10 °C under N_2 atmosphere. The frequency ranges from 100 mHz to 100 kHz. A polytetrafluoroethylene cell module with two copper electrodes was used to fix the membrane sample that was cut into a rectangle (1 cm × 5 cm). During testing, the module was immersed in the degassed ultrapure water for 2 h to reach an equilibrium state at a given temperature. The ion conductivity (σ) was calculated by

$$\sigma = \frac{l}{AR} \quad (6)$$

where l (cm) is the effective length of AEM sample between the two copper electrodes. A (cm^2) is the sectional area of AEM and can be calculated by the thickness and width of sample. R (Ω) is the AC impedance and was measured from electrochemical workstation. Furthermore, the alkaline stability was evaluated by comparing the hydroxide conductivity of AEMs before and after immersing in 1 M NaOH at 80 °C for 1 month.

2.7. Evaluation of H_2/O_2 fuel cell

The single cell performance was tested on a TE201 fuel cell system (Kunshan Sunlaite, China). The membrane electrode assembly (MEA) was prepared according to our previous work [28]. First, Pt/C catalyst (40 wt % Pt, Johnson Matthey), 5 wt % homemade ionomers (HPPO), DMF and ethanol were mixed to form the catalyst ink, which was sprayed evenly on both sides of the HPPO/PPO-C8 AEM (the thickness is ~23 μm) with a spray gun. The load of Pt on the AEM was 1.0 mg cm^{-2}.

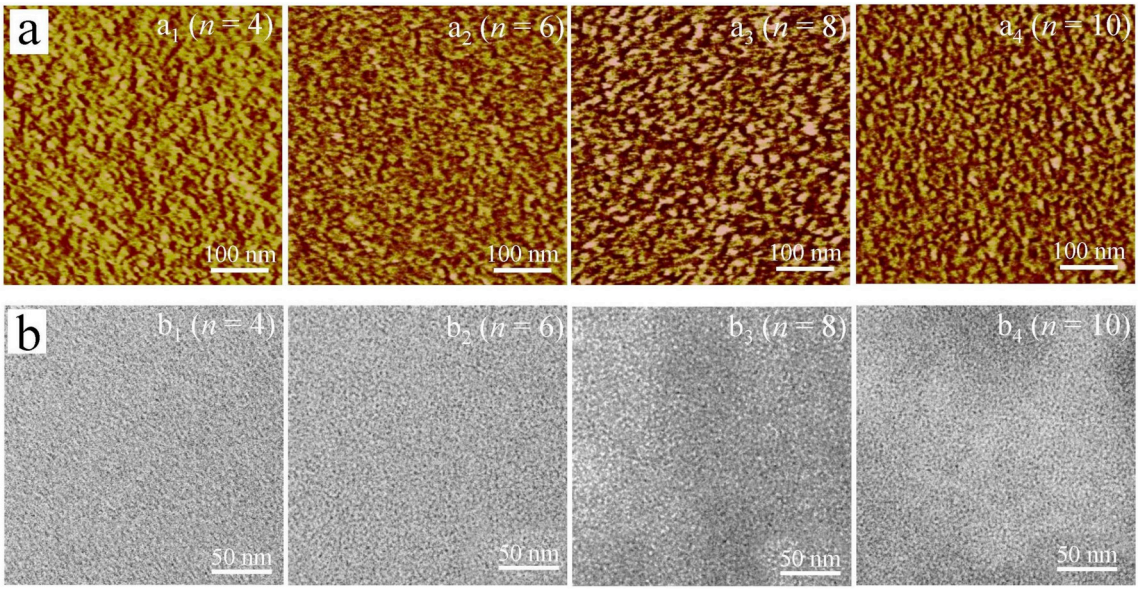

Fig. 4. Microphase separation structure of HPPO-C*n* AEMs, including (a) AFM phase images and (b) TEM images.

After that, the catalyst coated AEM was immersed in 1 M NaOH solution at 30 °C for 12 h to exchange Br with OH and then dried under vacuum at 60 °C for 12 h. Then, two pieces of carbon paper (2 cm × 2 cm) and a piece of catalyst coated AEM was assembled into the MEA. Finally, the MEA was installed into single cell system. The fuel cell performance was tested at 60 °C under 100% humidity and the hydrogen and oxygen flow rate were 200 mL min^{-1}.

3. Results and discussion

3.1. Preparation and chemical structure of HPPO-Cn AEMs

As shown in Fig. 2, the PPO was brominated first by using NBS to produce the HPPO. In the effect of AIBN, the NBS is easily to form free radicals that will take active hydrogens of phenyl methyl groups and further form the alkyl radicals [38]. Subsequently, the alkyl radicals capture the bromine of NBS to complete the brominating process. Chemical shifts of characteristic peaks show a one-to-one conformity with chemical structure in the ^{1}H NMR spectrum of resulting PPO-Br (Fig. S1), suggesting the PPO was brominated successfully. The brominating degree of PPO-Br is calculated to 35% from the integral of Ar–CH_2Br group (4.36 ppm) and Ar–CH_3 group (2.11 ppm). Then, the HPPO was prepared by partly grafting by the *N,N*-DQA, in which every *N,N*-DQA molecules will bring three quaternary ammonium groups to PPO backbones. The ^{1}H NMR spectrum of *N,N*-DQA is shown in Fig. S2. The chemical shift and integral area of characteristic peak is consistent with theoretical value which indicates that the pure target was obtained. Fig. 3a shows the ^{1}H NMR spectrum of the resulting HPPO. The peaks at 1.33 and 1.71 ppm are ascribed to methylene of side chains, indicating that the grafting is successful. The peak at 2.01 ppm is associated with methyl group linked to benzene ring. Further, the grafting ratio is 25% that calculated from the integral of methylene and methyl group.

The HPPO chains were crosslinked by primary diamines in the membrane formation. The resulting HPPO-C*n* AEMs were characterized by FT-IR, as shown in Fig. 3b. There are two obvious absorption peaks at 634 and 987 cm^{-1}, which are associated with the C–Br of PPO-Br [39]. After crosslinking, the above two peaks disappeared, suggesting the crosslinking took place. To evaluate the crosslinking degree, the gel fraction was measured by immersing the HPPO-C*n* AEMs in NMP at 80 °C for 24 h. As shown in Fig. 3c, the gel fractions of all the AEMs are over 80%, indicating the HPPO-C*n* AEMs were prepared successfully.

Since the hydrophobic crosslinker will restrict the membrane swelling greatly, the theoretical IEC of HPPO was controlled to a high value of 3.05 mmol g^{-1}. That is, the number mole of quaternary ammonium groups is constant in all the HPPO-C*n* AEMs. However, the measured IEC of the AEMs lightly decreases with increasing length of crosslinkers (Fig. 3c). This is because the addition of crosslinkers increased the weight of AEMs. The HPPO-C4 AEM has the highest IEC of 2.71 mmol g^{-1} due to the shortest crosslinker. On the contrary, the HPPO-C10 AEMs has the lowest IEC of 2.61 mmol g^{-1}.

3.2. Microphase separation structure of HPPO-Cn AEMs

The hydrophilic/hydrophobic separation structure is believed to benefit ion transport in the AEMs [40]. Fig. 3d display the SAXS profiles of HPPO-C*n* AEMs, which were used to estimate the size of ion domain in the AEMs. All the AEMs have distinct peaks located at 1.60, 1.49, 1.44 and 1.47 nm^{-1} for HPPO-C4, HPPO-C6 HPPO-C8 and HPPO-C10, respectively. Correspondingly, the inter-domain spacing (d) is 3.9, 4.2, 4.4 and 4.3 nm according to Bragg equation ($d = 2\pi\ q^{-1}$). That is, microphase separation should take place in the HPPO-C*n* AEMs, in which the HPPO-C8 AEM has the biggest ion domain. To confirm this result, AFM was used to observe surface properties of HPPO-C*n* AEMs, as shown in Fig. 4a. Obviously, all the AEMs show clear microphase separation structure, in which dark areas stand for hydrophilic domains that are composed of quaternary ammonium group and water. These hydrophilic domains are channels for ion transport in the AEMs. On the contrast, bright areas correspond to the hydrophobic domains that are consisted of hydrophobic backbone. Among these AEMs, the HPPO-C8 AEM has the largest ion clusters and well-connected ion channels. This is because the short crosslinker restrict mobility of backbones and thus depress self-assembly of backbones. However, the crosslinker is too long, possibly resulting in excessive aggregation of crosslinker, which is unfavorable for formation of phase separation structure in the AEMs [41].

The TEM further demonstrated the microphase separation structure of HPPO-C*n* AEMs. Fig. 4b show TEM images of inner microstructure of the AEMs, in which dark regions represent ion-rich domains while bright regions are associated with the backbone that are ion-poor domains. The larger the ion-rich domain is, the more favorable it is for ion transport in the AEMs. Comparing with other three AEMs, the HPPO-C8 AEM has more distinct microphase separation structure. This result is also corresponding to a change of the AEMs' density. As the length of

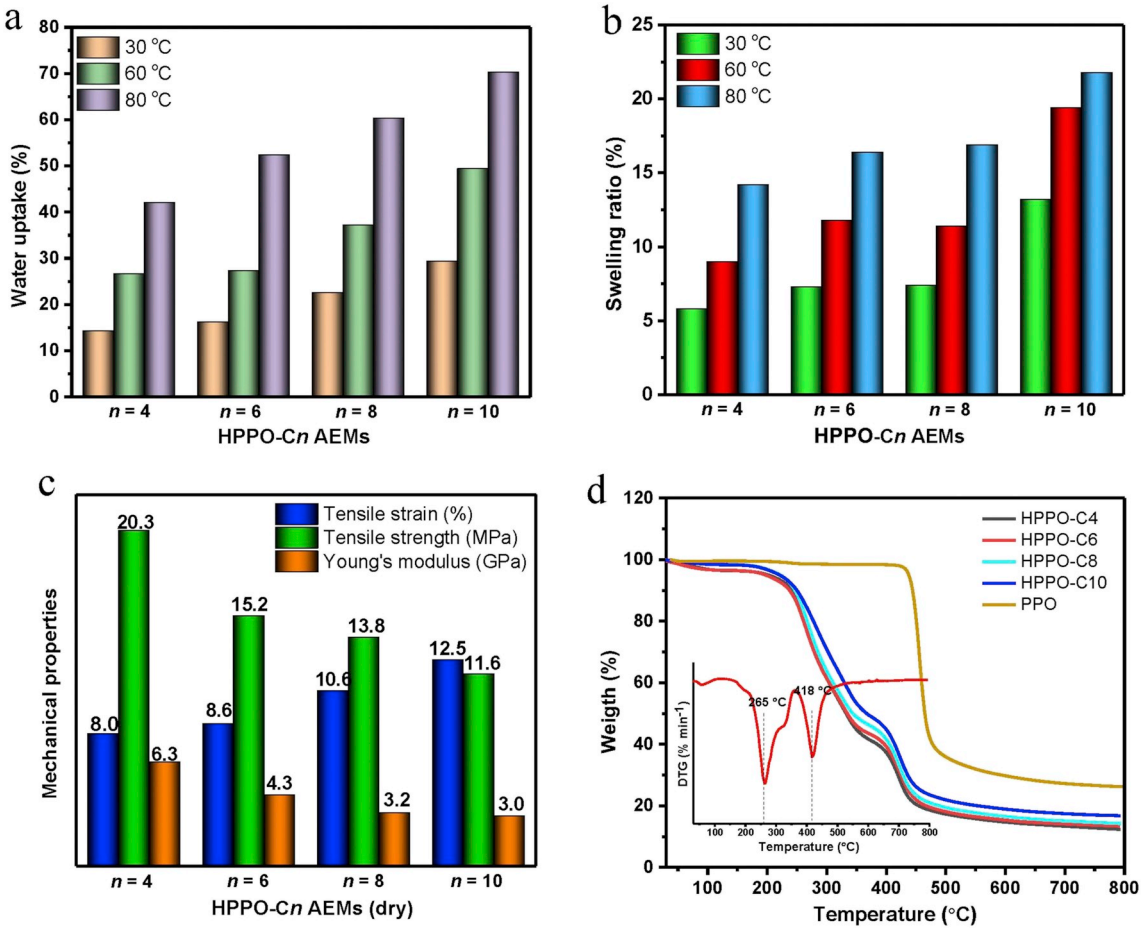

Fig. 5. Dimensional, mechanical and thermal stabilities of HPPO-C*n* AEMs. (a,b) The water uptake and swelling ratio of AEMs in water at 30, 60 and 80 °C. (c) Mechanical properties of dry AEMs, including tensile strain, tensile strength and Young's modulus. (d) TGA curves of AEMs (The inset is a DTG curve of HPPO-C4 AEMs).

crosslinkers increases, the density of HPPO-C*n* AEMs decreases first and then increases (Fig. S3). The HPPO-C8 AEM has the lowest density of 1.303 g cm^{-3} due to its large space between chains. From these, it is concluded that the 1,8-diaminooctane (C8) is the best to form the efficient ion channels in the HPPO-C*n* AEMs.

3.3. Dimensional, mechanical and thermal stabilities of HPPO-Cn AEMs

The dimensional stability is important for the AEMs, especially using in the fuel cells. Ideally, the AEMs should have good mechanical properties and dimensional stability. However, they usually exist trade-off relations with the ion conductivity. The high IEC always leads to great swelling in water, *i.e.*, high water uptake and high swelling ratio.

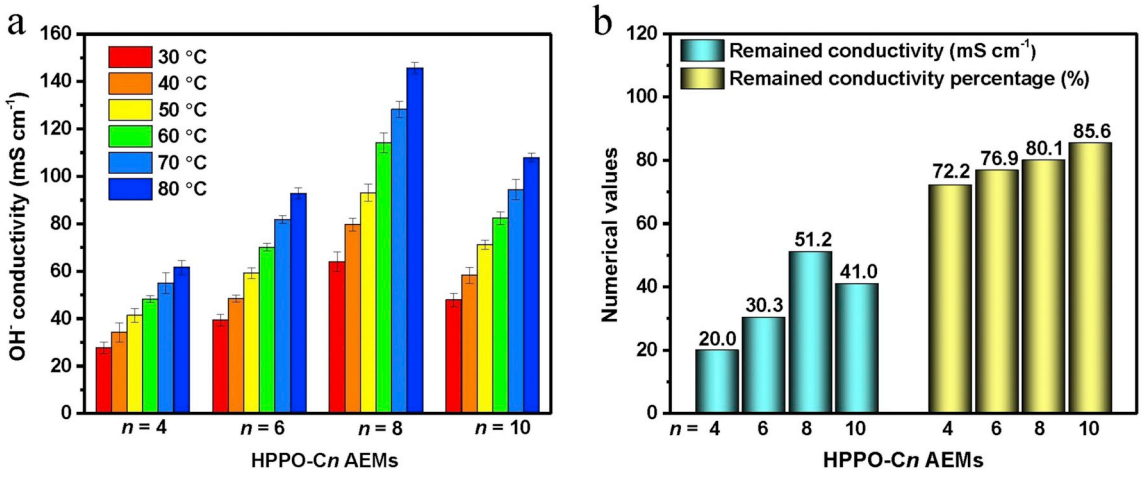

Fig. 6. Ion conductivity and alkaline resistance of HPPO-C*n* AEMs. (a) The hydroxide conductivity of AEMs in the range of 30–80 °C with an interval of 10 °C. (b) The remained hydroxide conductivity of AEMs after immersed in 1 M NaOH solution at 80 °C for 1 month.

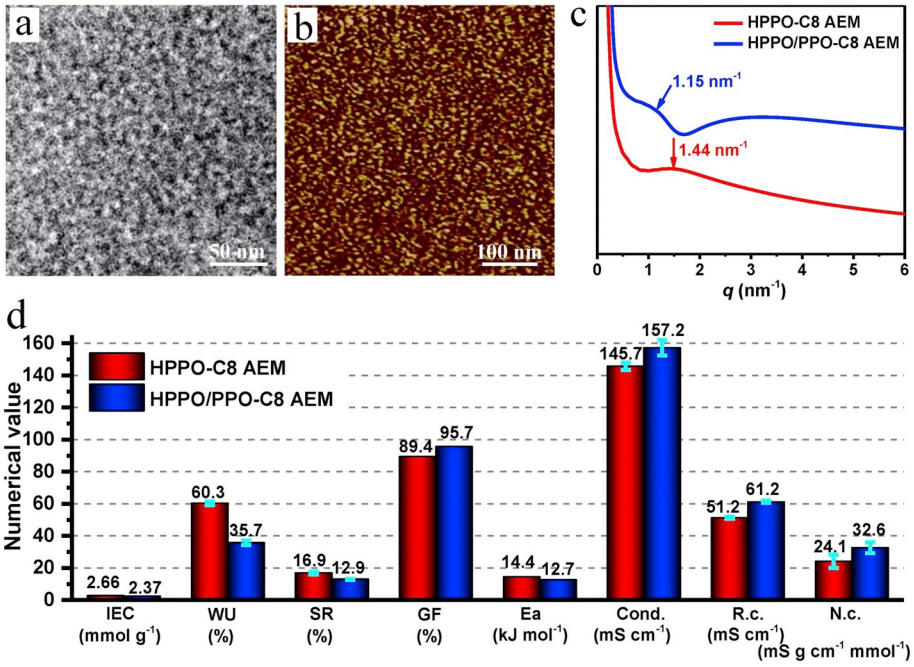

Fig. 7. Structure and performances of HPPO/PPO-C8 AEM with both hydrophobic crosslinker and hydrophobic chain. (a,b) TEM and AFM phase images of HPPO/PPO-C8 AEM. (c) SAXS profiles of HPPO-C8 and HPPO/PPO-C8 AEMs. (d) Performances of HPPO/PPO-C8 AEM comparing with the HPPO-C8 AEM, including IEC, water uptake (WU, 80 °C), swelling ratio (SR, 80 °C), gel fraction (GF), Ea, hydroxide conductivity (Cond. 80 °C), remained conductivity (R.c.) after alkaline test and normalized hydroxide conductivity (N.c.) (30 °C).

Suitable water uptake is essential for ion transport while the high swelling ratio is detrimental to the mechanical stability of AEMs. Fig. 5a and b displays the swelling properties of HPPO-C*n* AEMs at 30, 60 and 80 °C. The prepared AEMs have appropriate water uptake and low swelling ratio. Typically, the water uptake and swelling ratio increases from 42.1 to 70.3% and 14.2–21.8% at 80 °C with increasing length of crosslinkers, respectively. Thus, the HPPO-C*n* AEMs should have the good dimensional stability in the fuel cells.

Fig. 5c shows the mechanical properties of dry HPPO-C*n* AEMs in the Br form, including tensile strength, tensile strain and Young's modulus. All the AEMs exhibit the good mechanical properties. As the length of crosslinkers increases, the tensile strain increases from 8.0 to 12.5%, whereas the tensile strength and Young's modulus decreases from 20.3 to 11.6 MPa and 6.3 to 3.0 GPa, respectively. This is because the longer the crosslinker, the smaller the restriction of crosslinkers on the mobility of backbones, and the higher the water uptake. The high water uptake impairs interaction of polymer chains and finally results in the decrease of tensile strength [42]. The mechanical properties of the AEMs also were measured after swelling in water, as shown in Fig. S4. Contrastively, the swollen AEMs have higher tensile strain and lower tensile stress. This is because the backbones are more flexible and the force between atoms is weak in the swollen AEMs. Besides, absorbed water molecules acted as plasticizers will soften the AEMs and thus reduces the tensile stress [43].

The thermal stability of HPPO-C*n* AEMs was measured *via* thermos gravimetric analysis (TGA). As shown in Fig. 5d, there are two significant peaks in the TGA and differential thermal gravity (DTG) curves. The first peak is around 265 °C due to the degradation of quaternary ammonium groups and crosslinkers, which is greatly higher than the working temperature (~80 °C) of fuel cells. The second peak at 418 °C is attributed to the decomposing of PPO backbones. Therefore, the HPPO-C*n* AEMs have excellent thermal stability that can meet the application of fuel cells completely.

3.4. Ion conductivity and alkaline resistance of HPPO-Cn AEMs

The ion conductivity of HPPO-C*n* AEMs in the hydroxide form was measured from 30 to 80 °C with an interval of 10 °C, as shown in Fig. 6a. Novelty, as the length of crosslinkers increases, the hydroxide conductivity increases first and then decrease although the IEC decreases gradually. The change is attributed to microphase separation structure of the AEMs, as observed above. The HPPO-C8 AEM has the highest hydroxide conductivity of 145.7 mS cm^{-1} (80 °C) due to its developed ion channels. This result is contrary to most of AEMs, in which the ion conductivity usually increases with the IEC [38,44]. Compared with most of reported AEMs [45–47], the HPPO-C*n* AEMs have a moderate apparent activation energy of ion transport (14.26–15.37 kJ mol^{-1}) (Fig. S5).

Long-term alkaline stability is a challenge for the AEMs due to alkaline work environment. It is known that degradation mechanisms of quaternary ammonium are Hofmann elimination, nucleophilic substitution [48]. In this work, the prepared AEMs were immersed in 1 M NaOH solution at 80 °C for 1 month to evaluate their alkaline stability. The results are showed in Fig. 6b. All the AEMs exhibit the good alkaline stability that improves with increasing length of crosslinkers. The HPPO-C10 AEM has the best alkaline stability and remains 85.2% of initial hydroxide conductivity after immersed in harsh alkaline conditions for 1 month. The reason is that steric hindrance of long crosslinkers protect functional groups away from OH attacking [33]. Besides, water molecules will strongly bond to OH at alkaline conditions, and thus reduces nucleophilicity of OH to functional groups [49]. However, the working environment of AEM is not like the ex-suit conditions. Since water molecules are consumed continually in the cathode of AEMFC, the nucleophilicity of OH increased under water-starved environment, accelerating the degradation of functional groups [13]. Therefore, in the future, the alkaline stability of AEMs will be studied further, especially in the real operation environment and the relationship of water with alkaline stability [49,50].

3.5. Structure and performances of HPPO/PPO-C8 AEMs

Developing ion channels is believed to a direct method to promote ion transport [51]. To form more efficient ion channels, we introduced hydrophobic PPO chains into hydrophilic crosslinked network to adjust hydrophobic-hydrophilic property of HPPO-C8 AEM. As depicted in Fig. 2, the PPO-Br and HPPO was mixed in NMP, and then crosslinked by the 1,8-diaminooctane. As we expected, the as-formed HPPO/PPO-C8 AEM has a more distinct microphase separation structure compared

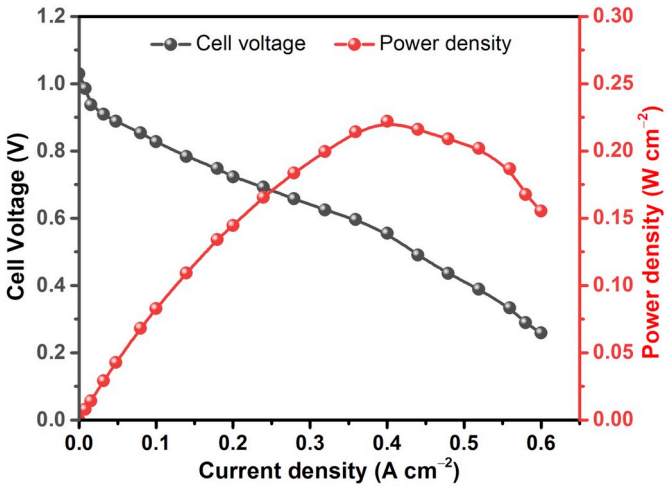

Fig. 8. Cell voltage and power density curves of H_2/O_2 fuel cell equipped with the HPPO/PPO-C8 AEM at 60 °C.

with the HPPO-C8 AEM, in which ion clusters are big and well connected (Fig. 7a and b). The result is confirmed by SAXS, as shown in Fig. 7c. The *d*-space of HPPO/PPO-C8 AEM is 5.4 nm that is bigger than 4.4 nm of HPPO-C8 AEM. Fig. S6 show the hydroxide conductivity of HPPO/PPO-C8 AEM, which linearly increases with the temperature in the range of 30–80 °C. The highest conductivity reaches 157.2 mS cm^{-1} at 80 °C.

To reveal advantages of introducing hydrophobic chains, a series of properties of HPPO/PPO-C8 and HPPO-C8 AEMs are compared in Fig. 7d. After introducing PPO chains, the IEC of HPPO/PPO-C8 decreases from 2.66 to 2.37 mmol g^{-1}. Apart from that, the water uptake and swelling ratio decreases from 60.3 to 35.7% and 16.9 to 12.9% respectively, but the hydroxide conductivity increases amazingly about 10%–157.2 mS cm^{-1} at 80 °C. This is due to the well-developed ion channels and low activation energy (12.68 kJ mol^{-1}). After alkaline test, the ionic conductivity of HPPO/PPO-C8 AEM decreases from 77.3 mS cm^{-1} to 61.2 mS cm^{-1} which is higher than that of PPO-C8 AEM (51.2 mS cm^{-1}) at 30 °C. Moreover, normalized hydroxide conductivity (conductivity per IEC) is improved from 24.1 to 32.6 mS g cm^{-1} mmol^{-1} that is higher than other crosslinked PPO-based AEMs reported recently (Fig. S7). From these, the prepared HPPO/PPO-C8 AEM shows high hydroxide conductivity and low swelling in water, and thus should has a wide application in the fuel cells.

The as-prepared HPPO/PPO-C8 AEM was applied in the H_2/O_2 fuel cell. The AEM in the hydroxide form was used to fabricate membrane electrode assembly (MEA). The single fuel cell was tested under humidified H_2 and O_2 at 60 °C. A gas flow rate was set as 200 mL min^{-1}. The resulting polarization curve and power density curve are showed in Fig. 8. The open circuit voltage is 1.03 V closing to the theoretical value of 1.23 V, indicating that there was little voltage lose caused by fuel crossover. The maximum power density achieves 222 mW cm^{-2} at a current density of 400 mA cm^{-2}. Although the achieved power density is less than that of most of AEMFCs in recent years (the highest is nearly 1.5 W cm^{-2}) [2], but still is higher than many crosslinked AEMs (Table S1). After optimizing the MEA and test condition, the performance of single fuel cell should be improved.

3.6. Trade-off relations in the crosslinked-type AEMs

It is well known that synthetic membranes usually suffer a ubiquitous trade-off between permeability and selectivity in gas separation [52]. For proton exchange membrane, there also exists an upper bound relation between ion conductivity and water uptake [53]. The water uptake is essential for the ion conductivity of AEMs. However, the excessive water uptake will reduce the ion conductivity due to ionic dilutes [50]. Here we collected experimental data of the hydroxide conductivity and swelling properties (*i.e.*, water uptake and swelling ratio) of crosslinked AEMs reported recently. The detail information is listed in Table S2. Obviously, the upper bound relation exists between ion conductivity and water uptake in the crosslinked AEMs, as shown in Fig. 9a. According to Robeson's report [53], this upper bound relation can be expressed by following formula: $water\ uptake = 516\sigma^{1.1855}$, where σ is the ion conductivity (S cm^{-1}). Usually, the high water uptake results in the high ion conductivity. However, it is a challenge to break the upper bound between ion conductivity and water uptake. Since the dimensional stability of AEMs is reciprocal to their swelling ratio, we plotted data points by using the reciprocal of swelling ration as X-values and the hydroxide conductivity as Y-values, as shown in Fig. 9b. Distinctly, the trade-off relation exists between the ion conductivity and the reciprocal of swelling ratio, and can be expressed by an equation: $1/swelling\ ratio = 202\sigma^{1.02}$.

An ideal AEM should has both high ion conductivity and high dimensional stability (*i.e.*, low swelling ratio). However, low swelling ratio always accompany low water uptake that has unfavorable to the ion transport. Amazingly, the HPPO/PPO-C8 AEM breaks the upper bound between ion conductivity and water uptake, and overcomes the trade-off between ion conductivity and dimensional stability in the

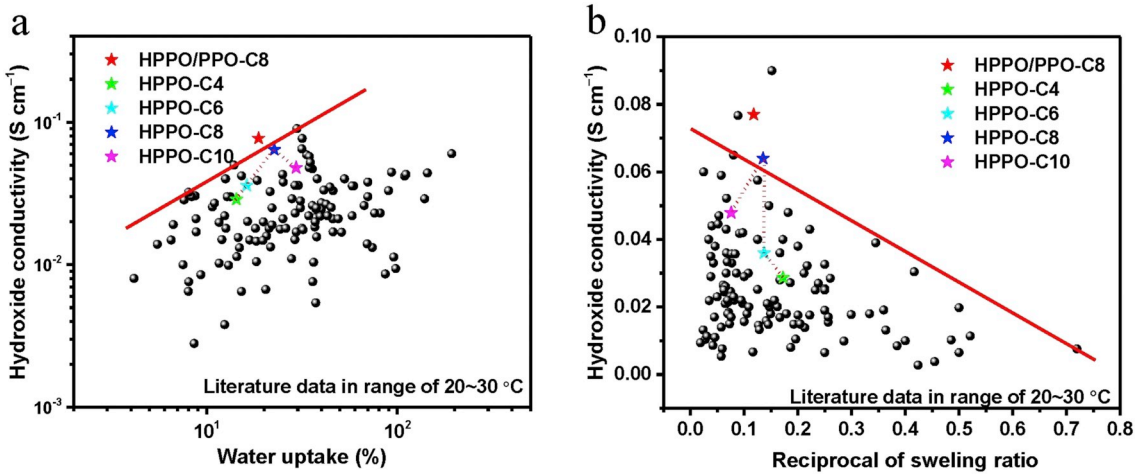

Fig. 9. Trade-off relations in the crosslinked AEMs. (a) The hydroxide conductivity for the crosslinked AEMs at a given level of water uptake is apparently limited by an upper bound type relationship. (b) The trade-off between the hydroxide conductivity and the dimensional stability (*i.e.*, reciprocal of swelling ratio) of crosslinked AEMs. The literature data are collected from the crosslinked AEMs published recently, and listed in Table S2.

crosslinked AEMs. Therefore, the presented strategy of dual hydrophobic modifications is favorable to develop the high-performance AEMs.

4. Conclusion

In summary, the novel strategy was developed to prepare the high-performance AEMs *via* dual hydrophobic modifications. The resulting PPO-based AEMs overcome the trade-off relation between ion conduction and dimensional stability of crosslinked AEMs, and thus have high ion conductivity as well as low swelling ratio. The alkyl diamines with various length were used to crosslink the HPPO. The formed HPPO-C*n* AEMs exhibit distinct microphase separation structure and good dimensional stability. As the length of crosslinkers increases, the hydroxide conductivity increases and then decreases. The AEM crosslinked by 1,8-diaminooctane achieved the maximum hydroxide conductivity (145.7 mS cm^{-1}, 80 °C). Subsequently, the hydrophobic PPO was introduced into the hydrophilic matrix to promote the microphase separation. The resulting HPPO/PPO-C8 AEM has the biggest ion clusters and the most well-connected ion channels, and show the highest hydroxide conductivity of 157.2 mS cm^{-1} at 80 °C. More importantly, this AEM has a moderate water uptake (35.7%) and a low swelling ratio (12.9%) at 80 °C, not only exceed the upper bound of the ion conductivity with the water uptake, but also break the trade-off between ion conductivity and dimensional stability of crosslinked AEMs. Furthermore, the AEM achieved the maximum power density of 222 mW cm^{-2} at 60 °C under a current density of 400 mA cm^{-2}, showing a great potential in application of fuel cells. The combination of high ion conductivity and low swelling makes the newly developed dual hydrophobic modifications attractive as a method to produce high-performance AEMs for fuel cell applications.

Declaration of competing interest

The authors declared that there is no conflict of interest.

Acknowledgements

This work was supported by the National Natural Science Foundation of China (No. 21676220, 21878253 and 21736009) and the Fundamental Research Funds for the Central Universities (No. 20720170032).

Appendix A. Supplementary data

Supplementary data to this article can be found online at https://doi.org/10.1016/j.memsci.2019.117521.

References

[1] N. Ziv, W.E. Mustain, D.R. Dekel, The effect of ambient carbon dioxide on anion-exchange membrane fuel cells, ChemSusChem 11 (2018) 1136–1150.
[2] D.R. Dekel, Review of cell performance in anion exchange membrane fuel cells, J. Power Sources 375 (2018) 158–169.
[3] S. Huo, J.W. Park, P. He, D. Wang, K. Jiao, Analytical modeling of liquid saturation jump effect for hydrogen alkaline anion exchange membrane fuel cell, Int. J. Heat Mass Transf. 112 (2017) 891–902.
[4] Z. Li, W. Wang, Y. Chen, C. Xiong, G. He, Y. Cao, H. Wu, M.D. Guiver, Z. Jiang, Constructing efficient ion nanochannels in alkaline anion exchange membranes by the in situ assembly of a poly(ionic liquid) in metal–organic frameworks, J. Mater. Chem. A 4 (2016) 2340–2348.
[5] H.-S. Dang, E.A. Weiber, P. Jannasch, Poly(phenylene oxide) functionalized with quaternary ammonium groups via flexible alkyl spacers for high-performance anion exchange membranes, J. Mater. Chem. A 3 (2015) 5280–5284.
[6] L.-c. Jheng, S.L.-c. Hsu, B.-y. Lin, Y.-l. Hsu, Quaternized polybenzimidazoles with imidazolium cation moieties for anion exchange membrane fuel cells, J. Membr. Sci. 460 (2014) 160–170.
[7] Z. Luo, Y. Gong, X. Liao, Y. Pan, H. Zhang, Nanocomposite membranes modified by graphene-based materials for anion exchange membrane fuel cells, RSC Adv. 6 (2016) 13618–13625.
[8] Z. Sun, J. Pan, J. Guo, F. Yan, The alkaline stability of anion exchange membrane for fuel cell applications: the effects of alkaline media, Adv. Sci. 5 (2018) 1800065.
[9] Y. He, L. Wu, J. Pan, Y. Zhu, X. Ge, Z. Yang, J. Ran, T. Xu, A mechanically robust anion exchange membrane with high hydroxide conductivity, J. Membr. Sci. 504 (2016) 47–54.
[10] T. Feng, B. Lin, S. Zhang, N. Yuan, F. Chu, M.A. Hickner, C. Wang, L. Zhu, J. Ding, Imidazolium-based organic–inorganic hybrid anion exchange membranes for fuel cell applications, J. Membr. Sci. 508 (2016) 7–14.
[11] T.P. Pandey, H.N. Sarode, Y. Yang, Y. Yang, K. Vezzù, V.D. Noto, S. Seifert, D. M. Knauss, M.W. Liberatore, A.M. Herring, A highly hydroxide conductive, chemically stable anion exchange membrane, poly(2,6 dimethyl 1,4 phenylene oxide)-b-poly(vinyl benzyl trimethyl ammonium), for electrochemical applications, J. Electrochem. Soc. 163 (2016) H513–H520.
[12] L. Liu, G. Sun, Simultaneously enhanced conductivity and dimensional stability of AAEM by crosslinked polymer microsphere with dense carrier sites, J. Appl. Polym. Sci. 135 (2018) 46715.
[13] D.R. Dekel, S. Willdorf, U. Ash, M. Amar, S. Pusara, S. Dhara, S. Srebnik, C. E. Diesendruck, The critical relation between chemical stability of cations and water in anion exchange membrane fuel cells environment, J. Power Sources 375 (2018) 351–360.
[14] C.E. Diesendruck, D.R. Dekel, Water – a key parameter in the stability of anion exchange membrane fuel cells, Curr. Opin. Electrochem. 9 (2018) 173–178.
[15] X.Q. Wang, C.X. Lin, Q.G. Zhang, A.M. Zhu, Q.L. Liu, Anion exchange membranes from hydroxyl-bearing poly(ether sulfone)s with flexible spacers via ring-opening grafting for fuel cells, Int. J. Hydrogen Energy 42 (2017) 19044–19055.
[16] Y.Z. Zhuo, A. Nan Lai, Q.G. Zhang, A.M. Zhu, M.L. Ye, Q.L. Liu, Highly ionic-conductive crosslinked cardo poly(arylene ether sulfone)s as anion exchange membranes for alkaline fuel cells, J. Membr. Sci. 491 (2015) 138–148.
[17] S. Gottesfeld, D.R. Dekel, M. Page, C. Bae, Y. Yan, P. Zelenay, Y.S. Kim, Anion exchange membrane fuel cells: current status and remaining challenges, J. Power Sources 375 (2018) 170–184.
[18] H.-S. Dang, P. Jannasch, Exploring different cationic alkyl side chain designs for enhanced alkaline stability and hydroxide ion conductivity of anion-exchange membranes, Macromolecules 48 (2015) 5742–5751.
[19] M. Tanaka, K. Fukasawa, E. Nishino, S. Yamaguchi, K. Yamada, H. Tanaka, B. Bae, K. Miyatake, M. Watanabe, Anion conductive block poly(arylene ether)s: synthesis, properties, and application in alkaline fuel cells, J. Am. Chem. Soc. 133 (2011) 10646–10654.
[20] C.X. Lin, X.Q. Wang, L. Li, F.H. Liu, Q.G. Zhang, A.M. Zhu, Q.L. Liu, Triblock copolymer anion exchange membranes bearing alkyl-tethered cycloaliphatic quaternary ammonium-head-groups for fuel cells, J. Power Sources 365 (2017) 282–292.
[21] E.A. Weiber, P. Jannasch, Polysulfones with highly localized imidazolium groups for anion exchange membranes, J. Membr. Sci. 481 (2015) 164–171.
[22] D. Chen, M.A. Hickner, Ion clustering in quaternary ammonium functionalized benzylmethyl containing poly(arylene ether ketone)s, Macromolecules 46 (2013) 9270–9278.
[23] R. He, P. Wen, H.-N. Zhang, S. Guan, G. Xie, L.-Z. Li, M.-H. Lee, X.-D. Li, In-situ photocrosslinked hydroxide conductive membranes based on photosensitive poly (arylene ether sulfone) block copolymers for anion exchange membrane fuel cells, J. Membr. Sci. 556 (2018) 73–84.
[24] J. Hou, Y. Liu, Q. Ge, Z. Yang, L. Wu, T. Xu, Recyclable cross-linked anion exchange membrane for alkaline fuel cell application, J. Power Sources 375 (2018) 404–411.
[25] J. Xue, L. Liu, J. Liao, Y. Shen, N. Li, UV-crosslinking of polystyrene anion exchange membranes by azidated macromolecular crosslinker for alkaline fuel cells, J. Membr. Sci. 535 (2017) 322–330.
[26] K.H. Lee, D.H. Cho, Y.M. Kim, S.J. Moon, J.G. Seong, D.W. Shin, J.-Y. Sohn, J. F. Kim, Y.M. Lee, Highly conductive and durable poly(arylene ether sulfone) anion exchange membrane with end-group cross-linking, Energy Environ. Sci. 10 (2017) 275–285.
[27] A. Amel, S.B. Smedley, D.R. Dekel, M.A. Hickner, Y. Ein-Eli, Characterization and chemical stability of anion exchange membranes cross-linked with polar electron-donating linkers, J. Electrochem. Soc. 162 (2015) F1047–F1055.
[28] C. Hu, Q. Zhang, C. Lin, Z. Lin, L. Li, F. Soyekwo, A. Zhu, Q. Liu, Multi-cation crosslinked anion exchange membranes from microporous Tröger's base copolymers, J. Mater. Chem. A 6 (2018) 13302–13311.
[29] S.P. Ertem, T.-H. Tsai, M.M. Donahue, W. Zhang, H. Sarode, Y. Liu, S. Seifert, A. M. Herring, E.B. Coughlin, Photo-cross-linked anion exchange membranes with improved water management and conductivity, Macromolecules 49 (2015) 153–161.
[30] C.X. Lin, Y.Z. Zhuo, E.N. Hu, Q.G. Zhang, A.M. Zhu, Q.L. Liu, Crosslinked side-chain-type anion exchange membranes with enhanced conductivity and dimensional stability, J. Membr. Sci. 539 (2017) 24–33.
[31] E. Abouzari-lotf, H. Ghassemi, M.M. Nasef, A. Ahmad, M. Zakeri, T.M. Ting, A. Abbasi, S. Mehdipour-Ataei, Phase separated nanofibrous anion exchange membranes with polycationic side chains, J. Mater. Chem. A 5 (2017) 15326–15341.
[32] Y. Liu, T.P. Pandey, H.N. Sarode, M.-C. Kuo, W. Zhang, R. Gupta, S. Galioto, A. G. Ozioko, S. Seifert, M.W. Liberatore, E.B. Coughlin, A.M. Herring, Thin, robust, and chemically stable photo-cross-linked anion exchange membranes based on a polychlorostyrene-b-polycyclooctene-b-polychlorostyrene ABA triblock polymer, Solid State Ion. 316 (2018) 135–142.
[33] N.W. Li, L.Z. Wang, M. Hickner, Cross-linked comb-shaped anion exchange membranes with high base stability, Chem. Commun. 50 (2014) 4092–4095.
[34] H.-S. Dang, P. Jannasch, Alkali-stable and highly anion conducting poly(phenylene oxide)s carrying quaternary piperidinium cations, J. Mater. Chem. A 4 (2016) 11924–11938.

[35] J. Ran, L. Wu, Y. Ru, M. Hu, L. Din, T. Xu, Anion exchange membranes (AEMs) based on poly(2,6-dimethyl-1,4-phenylene oxide) (PPO) and its derivatives, Polym. Chem. 6 (2015) 5809–5826.
[36] M.G. Marino, K.D. Kreuer, Alkaline stability of quaternary ammonium cations for alkaline fuel cell membranes and ionic liquids, ChemSusChem 8 (2015) 513–523.
[37] M.S. Cha, H.Y. Jeong, H.Y. Shin, S.H. Hong, T.-H. Kim, S.-G. Oh, J.Y. Lee, Y. T. Hong, Crosslinked anion exchange membranes with primary diamine-based crosslinkers for vanadium redox flow battery application, J. Power Sources 363 (2017) 78–86.
[38] N. Li, T. Yan, Z. Li, T. Thurn-Albrecht, W.H. Binder, Comb-shaped polymers to enhance hydroxide transport in anion exchange membranes, Energy Environ. Sci. 5 (2012) 7888–7892.
[39] L. Zhu, T.J. Zimudzi, Y. Wang, X. Yu, J. Pan, J. Han, D.I. Kushner, L. Zhuang, M. A. Hickner, Mechanically robust anion exchange membranes via long hydrophilic cross-linkers, Macromolecules 50 (2017) 2329–2337.
[40] J.-C. Chen, J.-A. Wu, K.-H. Chen, Synthesis and characterization of novel imidazolium-functionalized polyimides for high temperature proton exchange membrane fuel cells, RSC Adv. 6 (2016) 33959–33970.
[41] A.H.N. Rao, S. Nam, T.-H. Kim, Comb-shaped alkyl imidazolium-functionalized poly(arylene ether sulfone)s as high performance anion-exchange membranes, J. Mater. Chem. A 3 (2015) 8571–8580.
[42] J. Han, L. Zhu, J. Pan, T.J. Zimudzi, Y. Wang, Y. Peng, M.A. Hickner, L. Zhuang, Elastic long-chain multication cross-linked anion exchange membranes, Macromolecules 50 (2017) 3323–3332.
[43] T.D. Tap, D.D. Khiem, L.L. Nguyen, N.Q. Hien, L.Q. Luan, P.B. Thang, S.-i. Sawada, S. Hasegawa, Y. Maekawa, Humidity and temperature effects on mechanical properties and conductivity of graft-type polymer electrolyte membrane, Radiat. Phys. Chem. 151 (2018) 186–191.
[44] N. Li, Y. Leng, M.A. Hickner, C.Y. Wang, Highly stable, anion conductive, comb-shaped copolymers for alkaline fuel cells, J. Am. Chem. Soc. 135 (2013) 10124–10133.
[45] M. Liu, Z. Wang, J. Mei, J. Xu, L. Xu, H. Han, H. Ni, S. Wang, A facile functionalized routine for the synthesis of imidazolium-based anion-exchange membrane with excellent alkaline stability, J. Membr. Sci. 505 (2016) 138–147.
[46] C.X. Lin, Y.Z. Zhuo, A.N. Lai, Q.G. Zhang, A.M. Zhu, M.L. Ye, Q.L. Liu, Side-chain-type anion exchange membranes bearing pendent imidazolium-functionalized poly (phenylene oxide) for fuel cells, J. Membr. Sci. 513 (2016) 206–216.
[47] C.X. Lin, X.L. Huang, D. Guo, Q.G. Zhang, A.M. Zhu, M.L. Ye, Q.L. Liu, Side-chain-type anion exchange membranes bearing pendant quaternary ammonium groups via flexible spacers for fuel cells, J. Mater. Chem. A 4 (2016) 13938–13948.
[48] R. Espiritu, B.T. Golding, K. Scott, M. Mamlouk, Degradation of radiation grafted hydroxide anion exchange membrane immersed in neutral pH: removal of vinylbenzyl trimethylammonium hydroxide due to oxidation, J. Mater. Chem. A 5 (2017) 1248–1267.
[49] D.R. Dekel, M. Amar, S. Willdorf, M. Kosa, S. Dhara, C.E. Diesendruck, Effect of water on the stability of quaternary ammonium groups for anion exchange membrane fuel cell applications, Chem. Mater. 29 (2017) 4425–4431.
[50] Y. Zheng, U. Ash, R.P. Pandey, A.G. Ozioko, J. Ponce-González, M. Handl, T. Weissbach, J.R. Varcoe, S. Holdcroft, M.W. Liberatore, R. Hiesgen, D.R. Dekel, Water uptake study of anion exchange membranes, Macromolecules 51 (2018) 3264–3278.
[51] N. Li, M.D. Guiver, Ion transport by nanochannels in ion-Containing aromatic copolymers, Macromolecules 47 (2014) 2175–2198.
[52] H.B. Park, J. Kamcev, L.M. Robeson, M. Elimelech, B.D. Freeman, Maximizing the right stuff: the trade-off between membrane permeability and selectivity, Science 356 (2017) eaab0530.
[53] L. Robeson, H. Hwu, J. McGrath, Upper bound relationship for proton exchange membranes: empirical relationship and relevance of phase separated blends, J. Membr. Sci. 302 (2007) 70–77.